ACS OMEGA

Open Access

http://pubs.acs.org/journal/acsodf

Article

Hydroxyl-Incorporated Microporous Polymer Comprising 3D Triptycene for Selective Capture of CO_2 over N_2 and CH_4

Mosim Ansari, Aamir Hanif, Mahmoud M. Abdelnaby, Aasif Helal, and Mohd Yusuf Khan*

Cite This: *ACS Omega* 2025, 10, 2725−2734

Read Online

ACCESS | Metrics & More | Article Recommendations | Supporting Information

ABSTRACT: The rising CO_2 concentration in the atmosphere contributes significantly to global warming, necessitating effective carbon capture techniques. Amine-based solvents are widely employed for the chemisorption of CO_2, although they have drawbacks, such as degradation, corrosion, and high regeneration energy requirements. Physical adsorption of CO_2 utilizing microporous adsorbents is a viable alternative that offers excellent efficiency and selectivity for CO_2 capture. This work presents the facile one-pot synthesis of a 3D-triptycene-containing hyper-cross-linked microporous polymer (TBPP-OH) possessing hydroxyl groups. The presence of triptycene units in the TBPP-OH polymeric structure gives several desirable features, such as inherent microporosity, larger surface area, and improved thermal stability. TBPP-OH showed considerable microporosity ($\%V_{mic}$ = 70%), a larger BET-specific surface area (SA_{BET}) of 838 $m^2\ g^{-1}$, and good thermal stability (T_d = 372 °C and char yield > 60%) which makes it a promising adsorbent for CO_2 capture. A strong affinity for CO_2 was shown by TBPP-OH with Q_{st} of 32.9 kJ/mol demonstrating a superior CO_2 adsorption capacity of 2.77 mmol/g at 273 K and 1 bar pressure where the volume of the micropore plays a significant role. The selectivity values of CO_2 over N_2 and CH_4 for the polymer TBPP-OH were also estimated to be reasonably high indicating good potential for CO_2 separation in different applications. The mechanism of CO_2 adsorption was investigated by using Langmuir and dual-site Langmuir models.

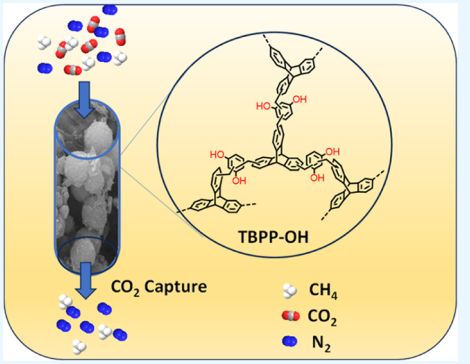

1. INTRODUCTION

The annual energy consumption is growing due to the continued rise of the world population and industrialization. CO_2 levels in the atmosphere continue to increase because fossil fuels are predominantly being used to produce energy.[1] Rising atmospheric concentration of carbon dioxide (CO_2) is recognized as the significant cause of global warming and its consequences such as climate change.[2] The latest statistics from 2024 shows that the atmospheric CO_2 content is higher than it has ever been in modern history, topping 420 ppm and continuing to rise. This corresponds to an approximate 50% rise since the start of the industrial age and an upsurge of around 14% since 2000 when the CO_2 concentration was already quite near 370 ppm. Consequently, "carbon capture and sequestration" (CCS) is the subject of extensive research in an attempt to lessen atmospheric CO_2 accumulation and its detrimental impacts on the ecosystem.[3] The wet scrubbing method in industry uses monoethanolamine (MEA) for the chemisorption of CO_2. However, there are serious drawbacks associated with this process, such as excessive consumption of energy and high regeneration costs, corrosion of equipments, and formation of harmful products due to chemical degradations of amine-based solvents.[4] In order to decrease the energy required for the regeneration process in comparison to present technical methods, it is essential that the adsorption of CO_2 is by physisorption with a higher capture efficiency and easy release. The utilization of porous adsorbents for carbon dioxide capture is a viable and efficient approach.[5,6] In contemporary research, the design of solid porous materials for effective CO_2 capture is of great importance.[7−9] Various porous materials have been investigated as potential materials for CO_2 capture such as adsorbents based on porous silica,[10] zeolite-based,[11] poly(ionic liquids),[12] porous carbons,[13−17] and metal−organic frameworks (MOFs).[18] Adsorbent design for CO_2 capture continues to advance in contemporary research. Recently, several smart adsorbents have been reported for controlled CO_2 capture, such as light-responsive adsorbents that can demonstrate selective adsorption with efficient regeneration.[19,20] However, over time, a novel group of polymeric materials known as porous organic polymers (POPs)—which have a persistent pore network and a large specific surface area—emerged for useful applications.[21−24] POPs have enormous promise for usage in numerous applications, such as catalysis, energy storage, and gas capture and separation, because of their higher porosity, design flexibility, larger surface area, low density, and exceptional

Received: September 14, 2024
Revised: November 16, 2024
Accepted: January 9, 2025
Published: January 15, 2025

physiochemical stability.[25] Hyper-cross-linked polymers (HCPs) are members of the POP family, which has garnered significant interest in recent years.[26−32] The Friedel−Crafts polymerization technique is typically used to design HCPs, which are amorphous polymers with strong cross-linking. Because of their facile synthesis, a large variety of aromatic monomers can be used to synthesize HCPs with different pore sizes and polymer properties. High chemical and thermal stability, larger surface area and microporosity, low density, efficient adsorption capabilities, simplicity in synthesis, affordability, and reusability are just a few of the many positive attributes of HCPs.[32] These unique features of HCPs, apart from other polymers, make them excellent choices for addressing environmental contamination[33] and energy issues.[30,34] In contemporary research, the design of efficient HCPs with desired adsorbent properties for CO_2 capture application is important. Some representative examples are as follows: Chen and co-workers reported the enhanced CO_2 capture in the hyper-cross-linked resin integrated microporous polymer where the adsorption capacity of CO_2 reaches 35.7 cm^3/g at 298 K;[35] Wang and colleagues reported the selective CO_2 capture in the presence of N_2 and CH_4 by triphenylamine-derived microporous HCPs;[36] and Zhang et al. also reported several benzyl alcohols-derived HCPs with a CO_2 uptake capacity of 1.86−1.96 mmol/g at 298 K and 1 bar. The desired adsorbent properties such as thermal and physiochemical stability, microporosity, and surface area may be obtained by employing 3D rigid robust motifs as monomers for the synthesis of high-performance HCPs. Triptycene is such a rigid robust and distinctive three-dimensional (3D) organic monomer comprising three phenyl rings arranged in a paddle wheel manner.[37] Internal free volume (IFV) and excellent thermal stability are known characteristics of its unique rigid and sturdy structure.[38] In recent decades, the utilization of materials comprising triptycene has been investigated for sensing,[39] electronics,[38] liquid crystal displays,[40] gas capture and separation,[41,42] host−guest chemistry,[43] and molecular machines.[44] In this work, we report the synthesis, characterization, and adsorption properties of a microporous polymer (TBPP-OH) comprising 3D triptycene motifs with ample hydroxyl group which was obtained via a facile one-step Friedel-Crafts cross-linking polymerization. TBPP-OH is predominantly microporous (pore size of less than 2 nm) with a larger BET-specific surface area of 838 m^2/g. The carbon dioxide adsorption capacity of TBPP-OH outperforms several porous polymeric adsorbents reported in the literature. We have also evaluated the CO_2/CH_4 and CO_2/N_2 selectivity values at different temperatures (273 and 298 K) up to 1 bar pressure. The selective capture of carbon dioxide over N_2 is essential for post-combustion CO_2 removal from flue gases, which typically contain more than 70% N_2 and around 10-15% CO_2. Additionally, it is crucial to separate CO_2 from CH_4 to increase the efficiency of natural and landfill gases which are richer in CH_4. TBPP-OH showed promising ability to selectively capture CO_2 at different temperatures. This showed that TBPP-OH is an efficient microporous polymer, with applications in selective CO_2 capture.

2. EXPERIMENTAL PART

2.1. Materials. Triptycene (98%), dimethoxymethane (99%), resorcinol (99%), and anhydrous $FeCl_3$ (99.99%) were purchased from Sigma-Aldrich. The following chemicals were obtained from Sigma-Aldrich and used without further purification: Anhydrous dichloroethane (DCE) (99.8%), methanol (99.6%), acetone (99.5%), and tetrahydrofuran (THF, 99.9%).

2.2. Synthesis of TBPP-OH. In a three-neck round-bottom flask (100 mL), triptycene (254 mg, 1 mmol), dimethoxymethane (348 μL, 3 mmol), resorcinol (110 mg, 1 mmol), and anhydrous $FeCl_3$ (648 mg, 4 mmol) were taken and subsequently, anhydrous DCE (30 mL) was added and refluxed for 24 h at constant stirring under an inert N_2 atmosphere. Then, the resulting residue solid thus formed was subjected to filtration and washed with DCE, distilled water, methanol, tetrahydrofuran (THF), and acetone. MeOH was used for 24 h to further purify the solid polymer using the Soxhlet apparatus. The resulting solid powder was then heated to 110 °C inside a vacuum oven for 24 h, yielding the desired polymer TBPP-OH (brown solid). Yield: 91%; FTIR: 3446 (broad, −OH), 3012, 2926 (−CH−), (Ar−C═C−, 1615−1467), 1378, 1262, 1223, 1183, 1097, 891, 822, 765 cm^{-1}.

2.3. Structural Characterizations. Using a Thermo Fisher Scientific (Nicolet 6700) instrument, we did Fourier transform infrared spectroscopy (FTIR) investigations to gain insight into the presence of different functional groups in TBPP-OH. A Thermo Scientific EscaLab 250Xi, system consisting of an Al Kα (1486.6 eV) source, was used for the X-ray photoelectron spectroscopy (XPS) analysis of TBPP-OH. Powder X-ray diffraction analysis (PXRD) was performed using a Rigaku Miniflex-II diffractometer that was connected to a Cu Kα anode (wavelength = 1.5416 Å). A 400 MHz Bruker instrument functioning at 125.65 MHz was used to perform the solid-state ^{13}C cross-polarization magic angle spinning (CP-MAS) NMR analysis. Thermogravimetric analysis (TGA) was done on a TA Q500 instrument under a N_2 flow (20 mL/min) at a 10 °C min^{-1} heating rate. The morphological properties of TBPP-OH were examined using a TESCAN-LYRA-3 (Czech Republic) field emission scanning electron microscopy (FESEM) instrument. A JEOL-JEM2100F instrument (Japan) was used to perform transmission electron microscopy (TEM) analysis at 200 kV acceleration voltage. Textural properties of TBPP-OH such as porosity and pore volumes were evaluated from N_2 isotherm data collected by utilizing a (Quantachrome Instruments) Quadrasorb SI instrument.

2.4. Gas Adsorption Experiment. Quantachrome Instrument (Quadrasorb SI) was used to obtain unary N_2, CO_2, and CH_4 isotherms at various temperatures. A dynamic vacuum (10^{-5} bar) at 120 °C for 12 h was used to pretreat about 0.2 g of the polymer samples prior to the isotherm measurements. The isotherm temperatures were maintained within the accuracy of ±1 °C by utilizing a circulation bath having an equimolar mixture of ethylene glycol and H_2O. The mechanism of CO_2 adsorption was elucidated by using the Langmuir model and dual-site Langmuir model (DSL), eqs 1 and 2, respectively, to fit the experimentally obtained isotherm data points.[45,46]

$$n^* = \frac{m_1 k_1 P}{1 + k_1 P} \tag{1}$$

$$n^* = \frac{m_1 k_1 P}{1 + k_1 P} + \frac{m_2 k_2 P}{1 + k_2 P} \tag{2}$$

https://doi.org/10.1021/acsomega.4c08460
ACS Omega 2025, 10, 2725−2734

Scheme 1. Synthesis of TBPP-OH

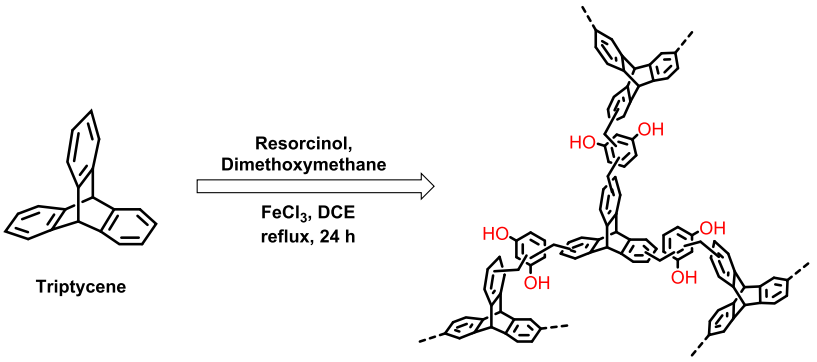

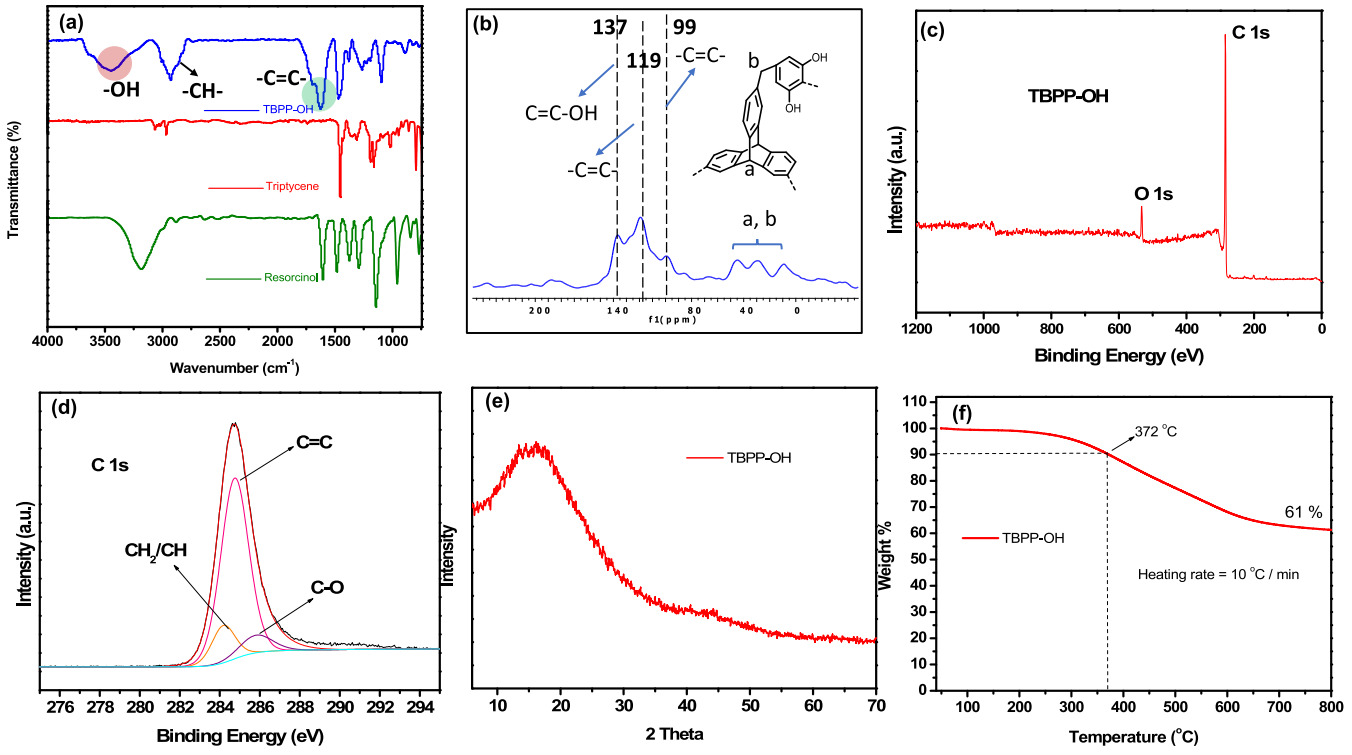

Figure 1. FTIR analysis (a), ^{13}C CP/MAS NMR (b), full-scan XPS spectrum (c), high-resolution C 1s spectrum (d), PXRD pattern (e), and TGA (f) of TBPP-OH.

where n^* is the predicted capacity (mmol/g), k_1 and k_2 are equilibrium constants (bar^{-1}) for sites of type 1 and type 2, respectively, and P is the pressure (bar).

Further, these isotherm results were used to calculate selectivity by ideal adsorbed solution theory (IAST selectivity) ($S_{1/2}$) for representative post-combustion flue gas (carbon dioxide = 15%) (nitrogen = 85%)[47] and biogas mixtures (50% CO_2 and 50% CH_4)[48] mixtures using eq 3.[49]

$$S_{1/2} = \frac{n_1}{n_2} \times \frac{p_2}{p_1} \tag{3}$$

where n_1 and n_2 are, respectively, the adsorption capacities (mmol/g) of component 1 and component 2 at p_1 and p_2, which represent the partial pressures of component 1 and component 2 in feed gas.

3. RESULTS AND DISCUSSION

3.1. Synthesis of TBPP-OH and Characterizations.

TBPP-OH polymer was prepared by Friedel−Crafts polymerization reaction using triptycene and resorcinol as monomers (Scheme 1). The polymer TBPP-OH is a brown-colored solid. The solubility analysis was performed in different solvents, and it was observed that TBPP-OH was insoluble in most of the common solvents like dichloromethane, tetrahydrofuran, dimethylformamide, and dimethyl sulfoxide (solubility analysis shown in Table S1). Structural characterizations of TBPP-OH were performed using ^{13}C CP/MAS NMR, FTIR, and XPS. FTIR analysis is shown in Figure 1a. The broad peak in the FTIR spectrum, which appears at around 3446 cm^{-1}, is ascribed to the polymer's −OH-functional groups.[42,50] Additionally, the peak observed at 2926 cm^{-1} corresponds to the characteristic −C−H stretching vibration of the aliphatic $-CH_2-$ groups, indicating successful cross-linking. Peaks resulting from characteristics aromatics' −C═C− stretching vibrations were observed at 1615 and 1467 cm^{-1}.[37]

https://doi.org/10.1021/acsomega.4c08460
ACS Omega 2025, 10, 2725−2734

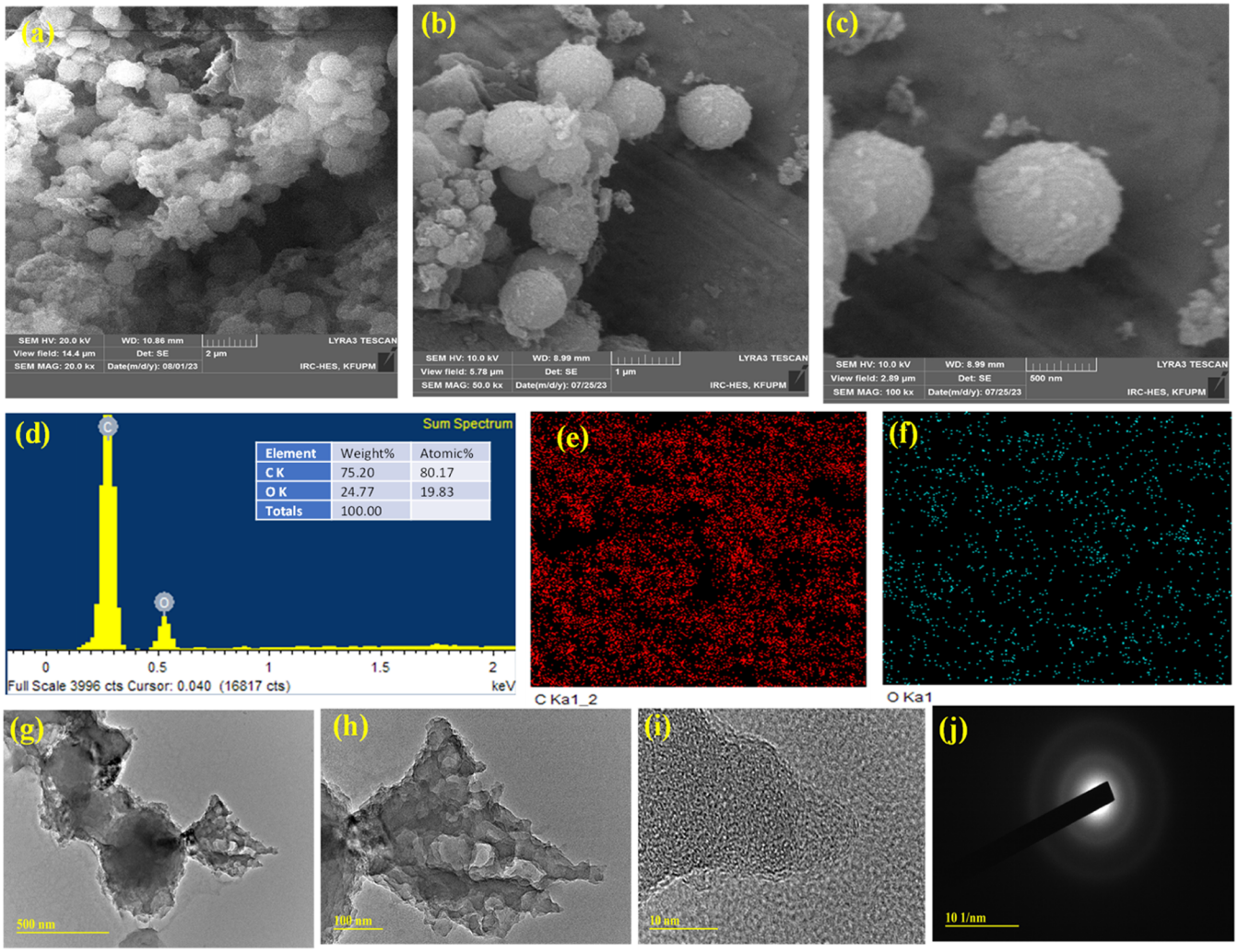

Figure 2. FESEM micrographs (a–c), EDS analysis (d), elemental mapping (e, f), and TEM images (g–j) of TBPP-OH.

Figure 1b displays the ^{13}C CP/MAS NMR spectrum of TBPP-OH. As expected, the broad peaks in the region of 140–99 ppm were attributed to the carbons of the aromatic rings. The peak observed at 137 ppm was assigned to hydroxyl-substituted aromatic carbon (C═C−OH). The peaks due to the bridgehead carbon of triptycene (−CH−) motifs and methylene carbons ($-CH_2-$) appeared at about 50–15 ppm. Therefore, ^{13}C CP/MAS NMR analysis clearly revealed the successful incorporation of resorcinol and triptycene units in the framework of the polymer TBPP-OH. TBPP-OH was also characterized by XPS analysis; the XPS analysis results are displayed in Figures 1c,d and S1. As can be seen in Figure 1c, the full-scan XPS spectrum of TBPP-OH exhibited two distinctly identifiable peaks at around 284 and 532 eV for C 1s and O 1s, respectively, indicating successful incorporation of resorcinol and triptycene. This conclusion was further supported by the high-resolution C 1s and O 1s photoemission spectra of TBPP-OH (Figures 1d and S1). The deconvoluted C 1s spectrum (Figure 1d) displays three distinct peaks at 285.81, 285.41, and 284.75 eV, respectively, ascribed to C−O, C═C, and CH_2/CH of TBPP-OH. The deconvoluted O 1s spectrum (Figure S1) shows one distinct peak at 532.52 attributed to hydroxyl oxygen of C═C−OH present in TBPP-OH.

Powder X-ray diffraction analysis (PXRD) of TBPP-OH shows a broad spectrum (Figure 1e), exhibiting its amorphous nature, which can be ascribed to the existence of rigid robust, and bulky triptycene motifs in the framework of polymer TBPP-OH.[42] The thermal characterization of TBPP-OH was determined by performing thermogravimetric analysis (TGA) (Figure 1f). Under an inert nitrogen environment, a given amount of sample of TBPP-OH was heated to 800 °C at a heating rate of 10 °C/min. TBPP-OH exhibited high thermal stability as indicated by its TGA experiment. The thermal degradation temperature (T_d) for TBPP-OH was 372 °C at which only 10% weight loss was registered. The char yield at 800 °C was observed to be 61%. The bearing of stiff, robust 3D triptycene molecules in TBPP-OH is attributed to the excellent thermal stability.[50−52]

Further to study the morphology of TBPP-OH, field emission scanning electron microscopy (FESEM) analysis was carried out. As shown in Figure 2a–c, FESEM micrographs reveal the formation of spherical shape aggregates that are roughly 0.5–1 μm in size. Similar morphology has been exhibited by other porous polymers made using Friedel-Crafts cross-linking polymerizations.[22,53] EDS and elemental mapping of TBPP-OH are also shown in Figure 2d–f. It is evident from SEM-EDS mappings of the polymer sample that TBPP-OH has a significantly higher O content of around 24% indicating

https://doi.org/10.1021/acsomega.4c08460
ACS Omega 2025, 10, 2725−2734

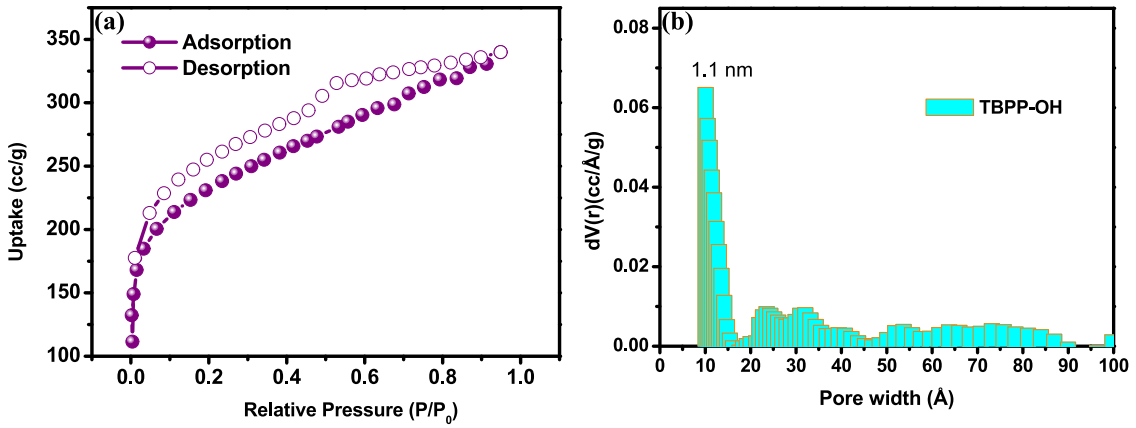

Figure 3. N_2 isotherm measured at 77 K (a) and PSD plot (b) of TBPP-OH.

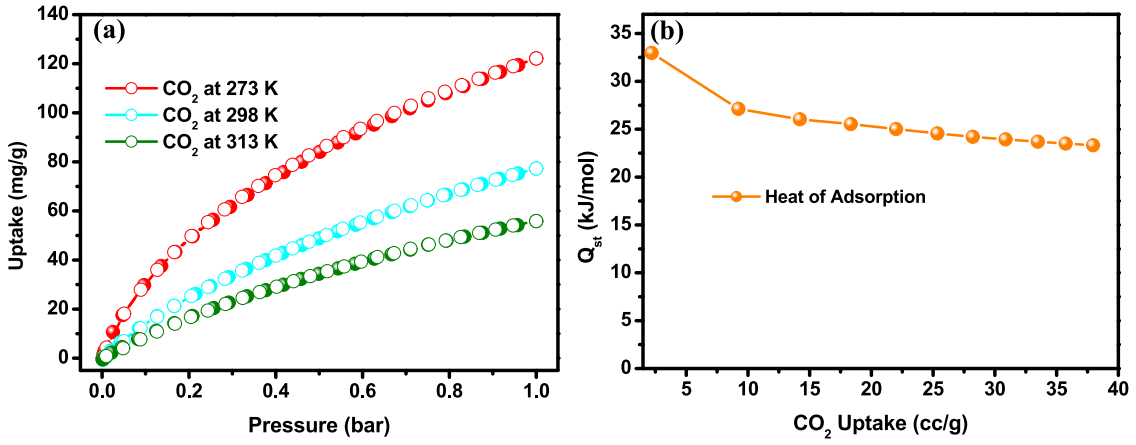

Figure 4. (a) Carbon dioxide uptake isotherms at different temperatures, filled sphere (adsorption) and empty sphere (desorption), and Q_{st} (heat of adsorption) (b) of TBPP-OH.

Table 1. Comparison of CO_2 Uptake and Selectivity of TBPP-OH with Other Reported Porous Polymers

material	CO_2 uptake at 1 bar (mg/g) 273 K	CO_2 uptake at 1 bar (mg/g) 298 K	CO_2 (Q_{st}) isosteric heat of adsorption (kJ/mol)	CO_2/N_2 selectivity 273 K (298 K) (IAST)	CO_2/N_2 selectivity 273 K (298 K) (Henry's law)	CO_2/CH_4 selectivity 273 K (298 K) (IAST)	CO_2/CH_4 selectivity 273 K (298 K) (Henry's law)	ref
TBPP-OH	122	77	32.9	37 (18)	33.7 (14)	4.2 (4.1)	7.4 (5.3)	this work
HCP1b	36.1	23.5	38.2	32.8				53
An-CPOP-1	61.5	57.1						59
PAF32	73	40	26					69
HCP-BA	84.6		27.4	28 (19)				70
HPIL-Cl-2	79	44	45	37				71
PCP-Cl	101.7	61.4	28.5	42 (34)				72
HCP-B	64.2	55.4						73
CB-PCP-1	90	53	35					74
TBP-1	51	35	33.7					75
STNP3	86	50	22					76
HMP-3	104	47						77
HPP-3	61	29.9	35					78

the presence of abundant hydroxyl groups. Additionally, this also demonstrates that resorcinol was successfully incorporated into the polymeric network of TBPP-OH. To further examine the morphology of TBPP-OH, TEM studies were performed, as shown in Figure 2g–j. TEM analysis of TBPP-OH showed nanosheet-like morphology and amorphous structure as evident from its HRTEM and SAED analysis.

3.2. Porous Properties of TBPP-OH. The nitrogen adsorption–desorption isotherm collected at 77 K and up to 1 bar pressure was used to evaluate the textural features, such as surface area, porosity, and pore volumes. As shown in Figure 3a, TBPP-OH displayed sharp uptake of N_2 at low pressures (P/P_0 = 0–0.01), indicating its microporous nature, while at high pressures, the isotherms slightly increased. This indicated the microporous nature of TBPP-OH. The pore size

https://doi.org/10.1021/acsomega.4c08460
ACS Omega 2025, 10, 2725−2734

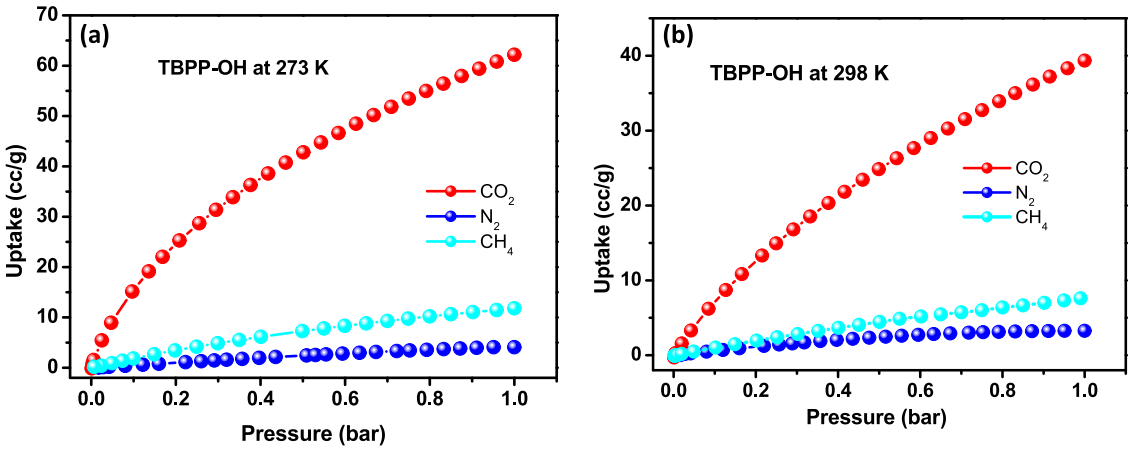

Figure 5. CO_2, N_2, and CH_4 adsorption isotherms at 273 K (a) and 298 K (b).

distribution plot (PSD) further confirms that TBPP-OH is considerably microporous (%V_{mic} = 70%) with the majority of pores in the region of 1.1 nm (Figure 3b). The microporous features of TBPP-OH may be ascribed to the existence of triptycene units with internal free volumes (IFV) and extensive cross-linking in the polymeric network. With a micropore volume of (V_{mic}) 0.346 $cm^3\ g^{-1}$ and a total pore volume (V_{tot}) of 0.491 $cm^3\ g^{-1}$, TBPP-OH demonstrated a larger BET-specific surface area (SA_{BET}) of 838 $m^2\ g^{-1}$ (BET plot, Figure S2). The observed SA_{BET} of TBPP-OH is higher compared to several other porous polymers such as oxygen-rich HCPs (up to 246.9 $m^2\ g^{-1}$),[53] HCTIn hyper-cross-linked networks (445−560 $m^2\ g^{-1}$),[54] phenanthroimidazole-based POPs (CPPs, 49−285 $m^2\ g^{-1}$),[55] HCPs based on pyrrolidinone (584 $m^2\ g^{-1}$),[56] nitrogen-rich POPs (POP101-104, 205−436 $m^2\ g^{-1}$),[57] and triazine-based porous polymers (308−456 $m^2\ g^{-1}$).[58]

3.3. CO_2 Capture Properties of TBPP-OH. To assess the CO_2-adsorption property of TBPP-OH, we performed CO_2 adsorption−desorption isotherms at various temperatures as displayed in Figure 4a. The hysteresis-free features of the CO_2 adsorption−desorption isotherms demonstrate the reversible CO_2 uptake capability of TBPP-OH (Figure 4a). The CO_2 uptake capacities of TBPP-OH are 122, 77, and 56 mg g^{-1} at 273, 298, and 313 K, respectively, and 1 bar of pressure (Table 1). The CO_2 capture efficiency at 273 K demonstrated by TBPP-OH is comparatively better than that of various other porous materials reported for CO_2 capture. A few representative examples are the capture capacities of tetraphenyl anthraquinone-based porous polymers (61.6−66.8 mg/g,),[59] nitrogen-rich porous material (97.8 mg/g),[60] triphenylamine- and triphenyl triazine-based COFs (92.38 mg g^{-1}),[61] triazine-based covalent imine framework (77.3 mg/g),[62] phthalazinone-based CTFs (84−103 mg/g),[63] microporous polymer network (6FA-PI-CL, 72.8 mg g^{-1}),[64] and bicarbazole-based porous polymers (CMPs, 92.3−93.5 mg g^{-1}).[65] Table 1 also displays the comparison of the CO_2 uptake performance of TBPP−OH with other literature-reported porous polymers. The carbon dioxide adsorption capacity of TBPP−OH at 298 K is also comparable or superior to many other porous polymers such as POP101-104 (40.65−38.49 mg g^{-1}),[57] An-CPOPs (57−61.6 mg g^{-1}),[59] TPT-COF-6 (65.65 mg g^{-1}),[61] TPA-TCIF(BD) (50.2 mg g^{-1}),[62] and CMPs (54.2−54.7 mg g^{-1})[65]

The excellent CO_2 uptake exhibited by TBPP-OH may be attributed to its highly microporous network formed by 3D triptycene and the presence of CO_2-philic −OH groups. The value of the isosteric heat of adsorption (Q_{st}) was also determined from the carbon dioxide uptake isotherms of TBPP-OH to further understanding of the CO_2-capturing mechanism (Figure 4b). The magnitude of Q_{st} was observed to be 32.9 kJ mol^{-1}, which suggested that the CO_2 adsorption by TBPP-OH is through physisorption. The observed Q_{st} is comparable to many other heteroatoms containing porous organic polymers, for instance, TF-PI-CL (28.6−30.2 kJ mol^{-1}),[64] melamine-based porous polyamides PTPAs (29.5−34.2 kJ mol^{-1}),[66] TPA-TCIF(BD) covalent imine frameworks (33.7 kJ mol^{-1}),[62] triazine-based nanoporous polymer (29.2−34.1 kJ mol^{-1}),[67] imine-based porous polymer, and PIN1−2 (30 kJ mol^{-1}),[68].

3.4. Selective Uptake of CO_2 over CH_4 and N_2 by TBPP-OH. After the successful CO_2 capture performance of TBPP-OH, we were further interested in gauging the CO_2/N_2 and CO_2/CH_4 selectivity for TBPP-OH at different temperatures. CO_2/N_2 separation is a crucial component for the capture of CO_2 from flue gases after combustion, which typically comprises more than 70% nitrogen and around 10-15% carbon dioxide. Further, it is important to separate CO_2 from CH_4 for the treatment of CH_4-rich gases, including biogas, which are often equimolar mixture of CO_2 and CH_4. Therefore, we assessed TBPP-OH's capability for the separation of landfill gas containing a CO_2/CH_4 mixture (50% CO_2:50% CH_4) and flue gas containing a CO_2 and N_2 mixture (15/85, v/v). Subsequently, to evaluate the selective CO_2 capture performance of TBPP-OH, the carbon dioxide, methane, and nitrogen uptake isotherms were collected at two different temperatures (273 and 298 K) and 1 bar pressure as displayed in Figure 5a,b. It was observed that TBPP-OH exhibited a significantly higher efficiency in capturing CO_2 compared to CH_4 and N_2; as a result, a higher uptake of CO_2 was accomplished in the two adsorption isotherms at temperatures 273 and 298 K. The CO_2/N_2 and CO_2/CH_4 selectivity curves of the adsorbent for feed gas simulating post-combustion CO_2 capture and biogas upgrading are given in Figure 6. The IAST method (Figure 6) was employed to measure the selectivity values for CO_2/CH_4 and CO_2/N_2. This method is commonly utilized to predict the selectivity for separation of a gas mixture by using experimental single-component adsorption isotherms. TBPP-OH displayed promising CO_2/N_2 selectivity of 37 at 273 K and 1 bar pressure (Table 1). In comparison to several porous polymers reported

https://doi.org/10.1021/acsomega.4c08460
ACS Omega 2025, 10, 2725−2734

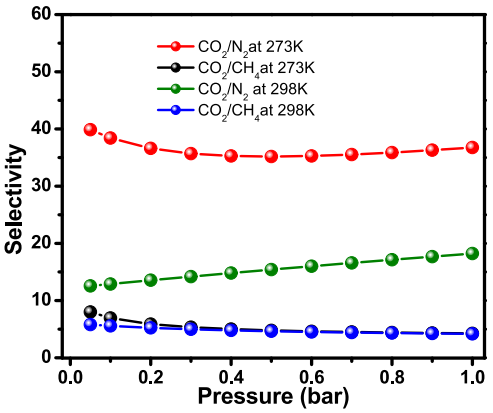

Figure 6. IAST selectivity curves for CO_2 (15%):N_2 (85%) and 50% CO_2:50% CH_4 composition.

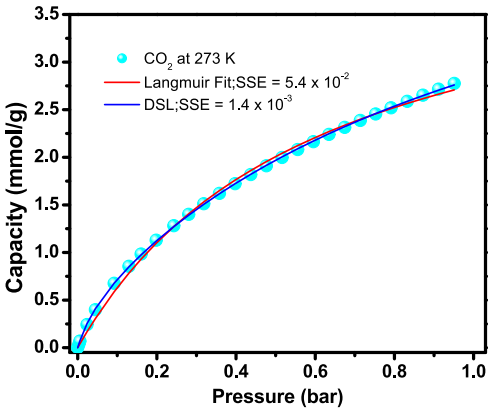

Figure 8. Langmuir and DSL model fit of the CO_2 isotherm at 273 K.

in the literature, the observed selectivity of CO_2/N_2 is either comparable to or better than, for example, HCP-0 (16.9),[79] HCP1b (32.8),[53] polyethyleneimine-grafted porous polymer (TCP-PEI, 34)[80] and porous polyamides PTPA-3 (31.6).[66]

At 298 K, the IAST selectivity value for CO_2/N_2 was 18 (Table 1). The selectivity values for CO_2/N_2 and CO_2/CH_4 were also measured using the Henry's law ratio of the initial slop method (Figure 7). The CO_2/N_2 and CO_2/CH_4 selectivities were, respectively, 33.7 and 7.4 at 273 K (Table 1). At a given temperature, the selectivity for CO_2/N_2 is better than CO_2/CH_4 selectivity, as CO_2 and N_2 show a greater difference in polarizability as compared to CO_2 and CH_4. Further, the decrease in selectivity with increasing temperature for both CO_2 over N_2 and CH_4 indicates that the adsorbent shows both better selectivity and capacity at 273 K. Moreover, the adsorption mechanism was elucidated by fitting the experimental adsorption data points with the Langmuir and dual-site Langmuir models (Figure 8). The experimental data can be predicted more appropriately using the dual-site Langmuir model, indicating two types of adsorption sites in the adsorbent. The adsorption and desorption isotherms are overlapping for all gases, indicating weak physisorption-type interactions and the possibility of adsorbent regeneration by a simple pressure/vacuum swing. Further, at both investigated temperatures, CO_2 capacity is the highest followed by CH_4 and N_2 is the least adsorbed. This is attributed to the highest polarizability (2.507 Å^3 vs 2.448 Å^3 for CH_4 and 1.710 Å^3 for N_2) and quadrupole moment (4.30 DÅ for CO_2 vs 1.54 DÅ and 0.02 DÅ for N_2 and CH_4) of CO_2 among the three gases which favors stronger physisorption interactions of CO_2 than the other two adsorbents. Further, CO_2 is a weakly acidic gas and may interact with the basic OH groups of the TBPP-OH through weak acid−base interactions. Moreover, though N_2 has a higher quadrupole moment than CH_4, CH_4 has higher polarizability than N_2, which favors its adsorption over N_2. For any gas, the adsorption decreases with increasing temperature also pointing to weak physisorption interactions existing between the adsorbate and adsorbent.

Estimating the recyclability of an adsorbent is essential for its practical use. As illustrated in Figure 9, the CO_2 uptake isotherms at 273 K and 1 bar for a maximum of 10 cycles were measured to evaluate the recyclability test. TBPP-OH showed promise as an adsorbent for CO_2 capture by adsorbing 120 mg/g of CO_2 without exhibiting any discernible reduction, even after 10 cycles without any activation treatment showing its potential for efficient CO_2 adsorption applications.

4. CONCLUSIONS

In summary, we presented the facile and one-pot preparation and characterization of a novel hyper-cross-linked microporous polymer based on 3D triptycene (TBPP-OH) adorned with hydroxyl functional groups. The presence of 3D stiff triptycene units in polymer TBPP-OH provides desirable features such as microporosity, higher surface area, and thermal stability. All of these properties in TBPP-OH render it a promising porous

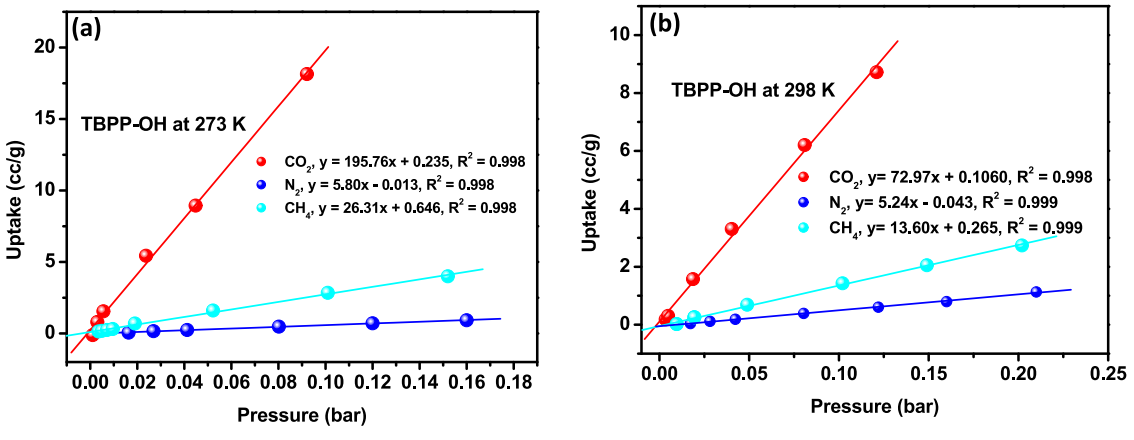

Figure 7. Initial gas uptake slopes of CO_2, N_2, and CH_4 for TBPP-OH at 273 K (a) and 298 K (b).

https://doi.org/10.1021/acsomega.4c08460
ACS Omega 2025, 10, 2725−2734

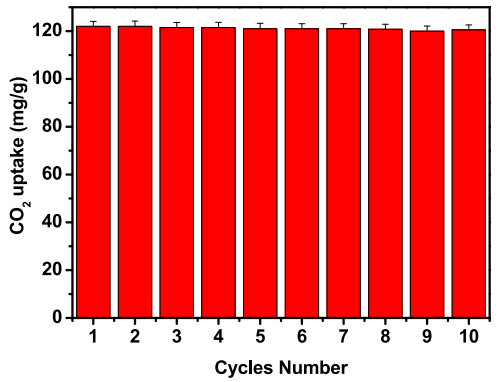

Figure 9. Recyclability performance of TBPP-OH as an adsorbent for capturing CO_2 at 273 K and 1 bar of pressure.

polymer for effective and selective CO_2 uptakes. TBPP-OH demonstrated a higher CO_2 uptake capacity of 122 mg g^{-1} at 273 K. The selectivity values for CO_2/N_2 were also observed to be reasonably high (up to 40). Considering the facile synthesis and ability to effectively and selectively adsorb CO_2 over CH_4 and N_2, TBPP-OH can be considered a potentially valuable material for environmental remediation applications. This work further motivates us and others to explore and synthesize OH-incorporated porous polymers connected with other stiff and aromatic motifs to improve the sorbent characteristics for practical applications given the desired structural features of TBPP-OH.

■ ASSOCIATED CONTENT

Supporting Information

The Supporting Information is available free of charge at https://pubs.acs.org/doi/10.1021/acsomega.4c08460.

BET-linear plot of polymer TBPP-OH, solubility test of polymer TBPP-OH, and high-resolution O 1s photoemission spectrum of TBPP-OH (PDF)

■ AUTHOR INFORMATION

Corresponding Author

Mohd Yusuf Khan − *Interdisciplinary Research Center for Hydrogen Technologies and Carbon Management (IRC-HTCM), King Fahd University of Petroleum & Minerals, Dhahran 31261, Saudi Arabia; Materials Science and Engineering Department, King Fahd University of Petroleum & Minerals, Dhahran 31261, Saudi Arabia;* orcid.org/0000-0002-1199-6232; Email: mykhan@kfupm.edu.sa

Authors

Mosim Ansari − *Interdisciplinary Research Center for Hydrogen Technologies and Carbon Management (IRC-HTCM), King Fahd University of Petroleum & Minerals, Dhahran 31261, Saudi Arabia*

Aamir Hanif − *Interdisciplinary Research Center for Hydrogen Technologies and Carbon Management (IRC-HTCM), King Fahd University of Petroleum & Minerals, Dhahran 31261, Saudi Arabia*

Mahmoud M. Abdelnaby − *Interdisciplinary Research Center for Hydrogen Technologies and Carbon Management (IRC-HTCM), King Fahd University of Petroleum & Minerals, Dhahran 31261, Saudi Arabia;* orcid.org/0000-0003-3434-8593

Aasif Helal − *Interdisciplinary Research Center for Hydrogen Technologies and Carbon Management (IRC-HTCM), King Fahd University of Petroleum & Minerals, Dhahran 31261, Saudi Arabia;* orcid.org/0000-0003-2013-5327

Complete contact information is available at: https://pubs.acs.org/10.1021/acsomega.4c08460

Notes

The authors declare no competing financial interest.

■ ACKNOWLEDGMENTS

The authors gratefully acknowledge the support provided by the Deanship of Research and the Interdisciplinary Research Center for Hydrogen Technologies and Carbon management (IRC-HTCM) for funding this work through the "project INHT2412" at King Fahd University of Petroleum & Minerals (KFUPM).They also acknowledge the Core Research Facility (CRF) at KFUPM for TEM analysis.

■ REFERENCES

(1) Dziejarski, B.; Serafin, J.; Andersson, K.; Krzyżyńska, R. CO_2 Capture Materials: A Review of Current Trends and Future Challenges. *Mater. Today Sustainability* **2023**, *24*, No. 100483.

(2) Abdullatif, Y.; Sodiq, A.; Mir, N.; Bicer, Y.; Al-Ansari, T.; El-Naas, M. H.; Amhamed, A. I. Emerging Trends in Direct Air Capture of CO2: A Review of Technology Options Targeting Net-Zero Emissions. *RSC Adv.* **2023**, *13*, 5687−5722.

(3) Dubey, A.; Arora, A. Advancements in Carbon Capture Technologies: A Review. *J. Cleaner Prod.* **2022**, *373*, No. 133932.

(4) Shi, Y. Q.; Zhu, J.; Liu, X. Q.; Geng, J. C.; Sun, L. B. Molecular Template-Directed Synthesis of Microporous Polymer Networks for Highly Selective CO2 Capture. *ACS Appl. Mater. Interfaces* **2014**, *6* (22), 20340−20349.

(5) Singh, G.; Lee, J.; Karakoti, A.; Bahadur, R.; Yi, J.; Zhao, D.; AlBahily, K.; Vinu, A. Emerging Trends in Porous Materials for CO2 Capture and Conversion. *Chem. Soc. Rev.* **2020**, *49* (13), 4360−4404.

(6) Shingdilwar, S.; Dolui, S.; Banerjee, S. Facile Fabrication of Functional Mesoporous Polymer Nanospheres for CO2 Capture. *Ind. Eng. Chem. Res.* **2022**, *61* (2), 1140−1147.

(7) Ansari, M.; Rehman, A. N.; Khan, A.; Khan, M. Y. Thermally Stable and High-Surface-Area Triptycene and Phenanthroline-Based Microporous Polymer for Selective CO2 Capture over CH4 and N2. *ACS Appl. Polym. Mater.* **2024**, *6* (7), 3996−4004.

(8) Sen, S.; Diab, R.; Al-Sayah, M. H.; Jabbour, R.; Equbal, A.; El-Kadri, O. M. Selective Carbon Dioxide Capture and Ultrahigh Iodine Uptake by Tetraphenylethylene-Functionalized Nitrogen-Rich Porous Organic Polymers. *ACS Appl. Polym. Mater.* **2024**, *6* (2), 1314−1324.

(9) Al-Ghourani, A.; Al-Hayek, M.; Al-Maythalony, B. A. In Situ Synthesis of Porphyrin-Based Hyper-Cross-Linked Sub-Nanometer Porous Polymer for Carbon Dioxide Adsorption Applications. *ACS Appl. Nano Mater.* **2024**, *7* (7), 6785−6790.

(10) Tumurbaatar, O.; Lazarova, H.; Popova, M.; Mitova, V.; Shestakova, P.; Koseva, N. CO2 Adsorption on the N-and P-Modified Mesoporous Silicas. *Nanomaterials* **2022**, *12* (7), 1224.

(11) Wang, X.; Chen, H.; Zhang, M.; Wang, C.; Wang, Y.; Bai, P.; Li, L.; Yan, W. Organic Template-Free Synthesis of K-SAPO-34 Zeolite for Efficient CO2 Separation. *Fuel* **2023**, *338*, No. 127233.

(12) Eftaiha, A. F.; Qaroush, A. K.; Hasan, A. K.; Assaf, K. I.; Al-Qaisi, F. M.; Melhem, M. E.; Al-Maythalony, B. A.; Usman, M. Cross-Linked, Porous Imidazolium-Based Poly(Ionic Liquid)s for CO2 Capture and Utilisation. *New J. Chem.* **2021**, *45* (36), 16452−16460.

(13) Liu, C.; Zhi, Y.; Yu, Q.; Tian, L.; Demir, M.; Colak, S. G.; Farghaly, A. A.; Wang, L.; Hu, X. Sulfur-Enriched Nanoporous Carbon: A Novel Approach to CO2 Adsorption. *ACS Appl. Nano Mater.* **2024**, *7* (5), 5434−5441.

(14) Shao, J.; Wang, J.; Yu, Q.; Yang, F.; Demir, M.; Altinci, O. C.; Umay, A.; Wang, L.; Hu, X. Unlocking the Potential of N-Doped Porous Carbon: Facile Synthesis and Superior CO2 Adsorption Performance. *Sep. Purif. Technol.* **2024**, *333*, No. 125891.
(15) Tian, L.; Zhi, Y.; Yu, Q.; Xu, Q.; Demir, M.; Colak, S. G.; Farghaly, A. A.; Wang, L.; Hu, X. Enhanced CO2 Adsorption Capacity in Highly Porous Carbon Materials Derived from Melamine-Formaldehyde Resin. *Energy Fuels* **2024**, *38* (14), 13186−13195.
(16) Hanif, A.; Aziz, Md. A.; Helal, A.; Abdelnaby, M. M.; Khan, A.; Theravalappil, R.; Khan, M. Y. CO2 Adsorption on Biomass-Derived Carbons from Albizia Procera Leaves: Effects of Synthesis Strategies. *ACS Omega* **2023**, *8* (39), 36228−36236.
(17) Hanif, A.; Aziz, M. A.; Helal, A.; Abdelnaby, M. M.; Qasem, M. A. A.; Khan, A.; Hakeem, A. S.; Al-Betar, A. F.; Khan, M. Y. CO2 Adsorption on Pore-Engineered Carbons Derived from Jute Sticks. *Chem. − Asian J.* **2023**, *18* (17), No. e202300481.
(18) Dong, Z.; Hu, W.; Liu, H.; Yang, Z.; Moitra, D.; Jiang, D.; Dai, S.; Hu, J. Z.; Wu, D.; Lin, H. Solvent-Treated Zirconium-Based Nanoporous UiO-66 Metal−Organic Frameworks for Enhanced CO2 Capture. *ACS Appl. Nano Mater.* **2023**, *6* (13), 12159−12167.
(19) Cheng, L.; Jiang, Y.; Qi, S.-C.; Liu, W.; Shan, S.-F.; Tan, P.; Liu, X.-Q.; Sun, L.-B. Controllable Adsorption of CO2 on Smart Adsorbents: An Interplay between Amines and Photoresponsive Molecules. *Chem. Mater.* **2018**, *30* (10), 3429−3437.
(20) Jiang, Y.; Shi, X.-C.; Tan, P.; Qi, S.-C.; Gu, C.; Yang, T.; Peng, S.-S.; Liu, X.-Q.; Sun, L.-B. Controllable CO2 Capture in Metal−Organic Frameworks: Making Targeted Active Sites Respond to Light. *Ind. Eng. Chem. Res.* **2020**, *59* (50), 21894−21900.
(21) Guo, C.; Chen, G.; Wang, N.; Wang, S.; Gao, Y.; Dong, J.; Lu, Q.; Gao, F. Construction of Multifunctional Histidine-Based Hypercrosslinked Hierarchical Porous Ionic Polymers for Efficient CO2 Capture and Conversion. *Sep. Purif. Technol.* **2023**, *312*, No. 123375.
(22) Hassan, A.; Goswami, S.; Alam, A.; Bera, R.; Das, N. Triptycene Based and Nitrogen Rich Hyper Cross Linked Polymers (TNHCPs) as Efficient CO2 and Iodine Adsorbent. *Sep. Purif. Technol.* **2021**, *257*, No. 117923.
(23) Zhao, L.; Liu, X.; Wang, S.; Li, Z.; Jiang, Y.; Xu, Y.; Yu, J.; Lei, Y. Low-Resistance and High-Tolerance Monolithic Spiro-Bifluorene-Based Conjugated Microporous Polymer for Co-Capture of PM and CO2 in Waste Gas. *Sep. Purif. Technol.* **2024**, *341*, No. 126825.
(24) Ashirov, T.; Song, K. S.; Coskun, A. Salt-Templated Solvothermal Synthesis of Dioxane-Linked Three-Dimensional Nanoporous Organic Polymers for Carbon Dioxide and Iodine Capture. *ACS Appl. Nano Mater.* **2022**, *5* (10), 13711−13719.
(25) Song, K. S.; Fritz, P. W.; Coskun, A. Porous Organic Polymers for CO2 Capture, Separation and Conversion. *Chem. Soc. Rev.* **2022**, *51*, 9831−9852.
(26) Ding, L.; Chanchaona, N.; Konstas, K.; Hill, M. R.; Fan, X.; Wood, C. D.; Lau, C. H. Synthesizing Hypercrosslinked Polymers with Deep Eutectic Solvents to Enhance CO2/N2 Selectivity. *ChemSusChem* **2024**, *17* (11), No. e202301602.
(27) Begni, F.; Lasseuguette, E.; Paul, G.; Bisio, C.; Marchese, L.; Gatti, G.; Ferrari, M.-C. Hyper-Cross-Linked Polymers with Sulfur-Based Functionalities for the Prevention of Aging Effects in PIM-1 Mixed Matrix Membranes. *ACS Appl. Polym. Mater.* **2023**, *5* (6), 4011−4018.
(28) Raza, S.; Abid, A.; Areej, I.; Nazeer, S.; Qureshi, A. K.; Tan, B. Fabrication of Phosphorus- and Nitrogen-Rich Inorganic−Organic Hybrid Hyper-Cross-Linked Polymers for CO2 and I2 Uptake. *ACS Appl. Polym. Mater.* **2024**, *6* (11), 6843−6851.
(29) Yang, S.; Zhong, Z.; Hu, J.; Wang, X.; Tan, B. Dibromomethane Knitted Highly Porous Hyper-Cross-Linked Polymers for Efficient High-Pressure Methane Storage. *Adv. Mater.* **2024**, *36* (19), No. 2307579.
(30) Song, W.; Tang, Y.; Moon, B. Y.; Liao, Q.; Xu, H.; Hou, Q.; Zhang, H.; Yu, D.-G.; Liao, Y.; Kim, I. Green Synthesis of Hypercrosslinked Polymers for CO2 Capture and Conversion: Recent Advances, Opportunities, and Challenges. *Green Chem.* **2024**, *26* (5), 2476−2504.
(31) Li, C.; Che, W.; Liu, S.-Y.; Liao, G. Hypercrosslinked Microporous Polystyrene: From Synthesis to Properties to Applications. *Mater. Today Chem.* **2023**, *29*, No. 101392.
(32) Tan, L.; Tan, B. Hypercrosslinked Porous Polymer Materials: Design, Synthesis, and Applications. *Chem. Soc. Rev.* **2017**, *46* (11), 3322−3356.
(33) Wang, J.; Wang, X.; Deng, Y.; Wu, T.; Chen, J.; Liu, J.; Xu, L.; Zang, Y. Preparation of an Electron-Rich Polyimide-Based Hypercrosslinked Polymer for High-Efficiency and Reversible Iodine Capture. *Polymer* **2023**, *267*, No. 125665.
(34) Moradi, M. R.; Torkashvand, A.; Ramezanipour Penchah, H.; Ghaemi, A. Amine Functionalized Benzene Based Hypercrosslinked Polymer as an Adsorbent for CO2/N2 Adsorption. *Sci. Rep.* **2023**, *13* (1), No. 9214.
(35) Wang, C.; Chen, X.; Yao, S.; Peng, F.; Xiong, L.; Guo, H.; Zhang, H.; Chen, X. Hyper-Cross-Linked Resin Modified by a Micropore Polymer for Gas Adsorption and Separation. *Langmuir* **2024**, *40* (24), 12465−12474.
(36) Wang, L.; Zhang, Y.; Jiang, H.; Wang, H. Carbonyl-Incorporated Aromatic Hyper-Cross-Linked Polymers with Microporous Structure and Their Functional Materials for CO2 Adsorption. *Ind. Eng. Chem. Res.* **2020**, *59* (36), 15955−15966.
(37) Ansari, M.; Das, N. Triptycene-Based Porous Photoluminescent Polymers with Dual Role: Efficient Capture of Carbon Dioxide and Sensitive Detection of Picric Acid. *Mater. Today Chem.* **2022**, *23*, No. 100723.
(38) Swager, T. M. Iptycenes in the Design of High Performance Polymers. *Acc. Chem. Res.* **2008**, *41* (9), 1181−1189.
(39) Ansari, M.; Hassan, A.; Alam, A.; Jana, A.; Das, N. Triptycene Based Fluorescent Polymers with Azo Motif Pendants: Effect of Alkyl Chain on Fluorescence, Morphology and Picric Acid Sensing. *React. Funct Polym.* **2020**, *146*, No. 104408.
(40) Song, M. H.; Park, B.; Shin, K. C.; Ohta, T.; Tsunoda, Y.; Hoshi, H.; Takanishi, Y.; Ishikawa, K.; Watanabe, J.; Nishimura, S.; Toyooka, T.; Zhu, Z.; Swager, T. M.; Takezoe, H. Effect of Phase Retardation on Defect-Mode Lasing in Polymeric Cholesteric Liquid Crystals. *Adv. Mater.* **2004**, *16* (9−10), 779−783.
(41) Ansari, M.; Bera, R.; Das, N. A Triptycene Derived Hypercrosslinked Polymer for Gas Capture and Separation Applications. *J. Appl. Polym. Sci.* **2022**, *139* (1), No. 51449.
(42) Ansari, M.; Hassan, A.; Alam, A.; Das, N. A Mesoporous Polymer Bearing 3D-Triptycene, − OH and Azo- Functionalities: Reversible and Efficient Capture of Carbon Dioxide and Iodine Vapor. *Microporous Mesoporous Mater.* **2021**, *323*, No. 111242.
(43) Ansari, M.; Mallik, S.; Jana, A.; Nayak, A.; Das, N. Photoresponsive Polymers with Dangling Triptycene Units as Efficient Receptor for Fullerene-C60. *J. Polym. Sci.* **2021**, *59*, 2959−2971.
(44) Ube, H.; Yamada, R.; Ishida, J. I.; Sato, H.; Shiro, M.; Shionoya, M. A Circularly Arranged Sextuple Triptycene Gear Molecule. *J. Am. Chem. Soc.* **2017**, *139* (46), 16470−16473.
(45) Foo, K. Y.; Hameed, B. H. Insights into the Modeling of Adsorption Isotherm Systems. *Chem. Eng. J.* **2010**, *156*, 2−10.
(46) Hanif, A.; Dasgupta, S.; Nanoti, A. Facile Synthesis of High-Surface-Area Mesoporous MgO with Excellent High-Temperature CO2 Adsorption Potential. *Ind. Eng. Chem. Res.* **2016**, *55* (29), 8070−8078.
(47) Andersen, A.; Divekar, S.; Dasgupta, S.; Cavka, J. H.; Aarti, A.; Nanoti, A.; Spjelkavik, A.; Goswami, A. N.; Garg, M. O.; Blom, R. On the Development of Vacuum Swing Adsorption (VSA) Technology for Post-Combustion CO2 Capture. *Energy Procedia* **2013**, *37*, 33−39.
(48) Arya, A.; Divekar, S.; Rawat, R.; Gupta, P.; Garg, M. O.; Dasgupta, S.; Nanoti, A.; Singh, R.; Xiao, P.; Webley, P. A. Upgrading Biogas at Low Pressure by Vacuum Swing Adsorption. *Ind. Eng. Chem. Res.* **2015**, *54* (1), 404−413.
(49) Singh, N.; Dalakoti, S.; Wamba, H. N.; Chauhan, R.; Divekar, S.; Dasgupta, S.; Aarti. Preparation of Cu-BTC MOF Extrudates for CH4 Separation from CH4/N2 Gas Mixture. *Microporous Mesoporous Mater.* **2023**, *360*, No. 112723.

https://doi.org/10.1021/acsomega.4c08460
ACS Omega 2025, 10, 2725−2734

(50) Ansari, M.; Alam, A.; Bera, R.; Hassan, A.; Goswami, S.; Das, N. Synthesis, Characterization and Adsorption Studies of a Novel Triptycene Based Hydroxyl Azo-Nanoporous Polymer for Environmental Remediation. *J. Environ. Chem. Eng.* **2020**, *8* (2), No. 103558.
(51) Alam, A.; Bera, R.; Ansari, M.; Hassan, A.; Das, N. Triptycene-Based and Amine-Linked Nanoporous Networks for Efficient CO2 Capture and Separation. *Front. Energy Res.* **2019**, *7*, No. 141, DOI: 10.3389/fenrg.2019.00141.
(52) Ansari, M.; Mallik, S.; Mondal, S.; Bera, R.; Jana, A.; Nayak, A.; Das, N. Triptycene-Based Fluorescent Polymers with Pendant Alkyl Chains: Interaction with Fullerenes and Morphology of Thin Films. *Polym. Int.* **2019**, *68* (3), 481−493.
(53) Shao, L.; Liu, N.; Wang, L.; Sang, Y.; Wan, H.; Zhan, P.; Zhang, L.; Huang, J.; Chen, J. Facile Preparation of Oxygen-Rich Porous Polymer Microspheres from Lignin-Derived Phenols for Selective CO2 Adsorption and Iodine Vapor Capture. *Chemosphere* **2022**, *288*, No. 132499.
(54) Wen, J.; Xiao, L.; Sun, T.; Lei, Z.; Chen, H.; Li, H. Fine Tuning of Specific Surface Area and CO2 Capture Performance in Hyper-Cross-Linked Heterocyclic Networks with Tetrazinyl Linker. *Microporous Mesoporous Mater.* **2021**, *319*, No. 111069.
(55) Monterde, C.; Navarro, R.; Iglesias, M.; Sánchez, F. Fluorine-Phenanthroimidazole Porous Organic Polymer: Efficient Microwave Synthesis and Photocatalytic Activity. *ACS Appl. Mater. Interfaces* **2019**, *11* (3), 3459−3465.
(56) Li, X.; Chen, G.; Ma, J.; Jia, Q. Pyrrolidinone-Based Hypercrosslinked Polymers for Reversible Capture of Radioactive Iodine. *Sep. Purif. Technol.* **2019**, *210*, 995−1000.
(57) Abdelnaby, M. M.; Aliyu, M.; Nemitallah, M. A.; Alloush, A. M.; Mahmoud, E. H. M.; Ossoss, K. M.; Zeama, M.; Dowaidar, M. Design and Synthesis of N-Doped Porous Carbons for the Selective Carbon Dioxide Capture under Humid Flue Gas Conditions. *Polymers* **2023**, *15* (11), 2475.
(58) Geng, T.; Zhang, W.; Zhu, Z.; Kai, X. Triazine-Based Conjugated Microporous Polymers Constructing Triphenylamine and Its Derivatives with Nitrogen as Core for Iodine Adsorption and Fluorescence Sensing I2. *Microporous Mesoporous Mater.* **2019**, *273*, 163−170.
(59) Mohamed, M. G.; Zhang, X.; Mansoure, T. H.; El-Mahdy, A. F. M.; Huang, C.-F.; Danko, M.; Xin, Z.; Kuo, S.-W. Hypercrosslinked Porous Organic Polymers Based on Tetraphenylanthraquinone for CO2 Uptake and High-Performance Supercapacitor. *Polymer* **2020**, *205*, No. 122857.
(60) Cui, Y.; Du, J.; Liu, Y.; Yu, Y.; Wang, S.; Pang, H.; Liang, Z.; Yu, J. Design and Synthesis of a Multifunctional Porous N-Rich Polymer Containing s-Triazine and Tröger's Base for CO2 Adsorption, Catalysis and Sensing. *Polym. Chem.* **2018**, *9* (19), 2643−2649.
(61) El-Mahdy, A. F. M.; Kuo, C. H.; Alshehri, A.; Young, C.; Yamauchi, Y.; Kim, J.; Kuo, S. W. Strategic Design of Triphenylamine- and Triphenyltriazine-Based Two-Dimensional Covalent Organic Frameworks for CO2 Uptake and Energy Storage. *J. Mater. Chem. A* **2018**, *6*, 19532−19541.
(62) Puthiaraj, P.; Kim, H. S.; Yu, K.; Ahn, W. S. Triphenylamine-Based Covalent Imine Framework for CO2 Capture and Catalytic Conversion into Cyclic Carbonates. *Microporous Mesoporous Mater.* **2020**, *297*, No. 110011.
(63) Yuan, K.; Liu, C.; Zong, L.; Yu, G.; Cheng, S.; Wang, J.; Weng, Z.; Jian, X. Promoting and Tuning Porosity of Flexible Ether-Linked Phthalazinone-Based Covalent Triazine Frameworks Utilizing Substitution Effect for Effective CO2 Capture. *ACS Appl. Mater. Interfaces* **2017**, *9* (15), 13201−13212.
(64) Song, N.; Wang, T.; Yao, H.; Ma, T.; Shi, K.; Tian, Y.; Zou, Y.; Zhu, S.; Zhang, Y.; Guan, S. Construction and Carbon Dioxide Capture of Microporous Polymer Networks with High Surface Area Based on Cross-Linkable Linear Polyimides. *Polym. Chem.* **2019**, *10* (33), 4611−4620.
(65) Yuan, Y.; Huang, H.; Chen, L.; Chen, Y. N,N′-Bicarbazole: A Versatile Building Block toward the Construction of Conjugated Porous Polymers for CO2 Capture and Dyes Adsorption. *Macromolecules* **2017**, *50* (13), 4993−5003.
(66) Shao, L.; Liu, M.; Sang, Y.; Huang, J. One-Pot Synthesis of Melamine-Based Porous Polyamides for CO2 Capture. *Microporous Mesoporous Mater.* **2019**, *285*, 105−111.
(67) Xiong, S.; Fu, X.; Xiang, L.; Yu, G.; Guan, J.; Wang, Z.; Du, Y.; Xiong, X.; Pan, C. Liquid Acid-Catalysed Fabrication of Nanoporous 1,3,5-Triazine Frameworks with Efficient and Selective CO2 Uptake. *Polym. Chem.* **2014**, *5* (10), 3424−3431.
(68) Popp, N.; Homburg, T.; Stock, N.; Senker, J. Porous Imine-Based Networks with Protonated Imine Linkages for Carbon Dioxide Separation from Mixtures with Nitrogen and Methane. *J. Mater. Chem. A* **2015**, *3* (36), 18492−18504.
(69) Jing, X.; Zou, D.; Cui, P.; Ren, H.; Zhu, G. Facile Synthesis of Cost-Effective Porous Aromatic Materials with Enhanced Carbon Dioxide Uptake. *J. Mater. Chem. A* **2013**, *1* (44), 13926−13931.
(70) Luo, Y.; Zhang, S.; Ma, Y.; Wang, W.; Tan, B. Microporous Organic Polymers Synthesized by Self-Condensation of Aromatic Hydroxymethyl Monomers. *Polym. Chem.* **2013**, *4* (4), 1126−1131.
(71) Sang, Y.; Huang, J. Benzimidazole-Based Hyper-Cross-Linked Poly(Ionic Liquid)s for Efficient CO2 Capture and Conversion. *Chem. Eng. J.* **2020**, *385*, No. 123973.
(72) Buyukcakir, O.; Je, S. H.; Choi, D. S.; Talapaneni, S. N.; Seo, Y.; Jung, Y.; Polychronopoulou, K.; Coskun, A. Porous Cationic Polymers: The Impact of Counteranions and Charges on CO2 Capture and Conversion. *Chem. Commun.* **2016**, *52* (5), 934−937.
(73) Huang, J.; Zhu, J.; Snyder, S. A.; Morris, A. J.; Turner, S. R. Nanoporous Highly Crosslinked Polymer Networks with Covalently Bonded Amines for CO2 Capture. *Polymer* **2018**, *154*, 55−61.
(74) Dani, A.; Crocellà, V.; Magistris, C.; Santoro, V.; Yuan, J.; Bordiga, S. Click-Based Porous Cationic Polymers for Enhanced Carbon Dioxide Capture. *J. Mater. Chem. A* **2017**, *5* (1), 372−383.
(75) Bera, R.; Mondal, S.; Das, N. Nanoporous Triptycene Based Network Polyamides (TBPs) for Selective CO2 Uptake. *Polymer* **2017**, *111*, 275−284.
(76) Alam, A.; Hassan, A.; Bera, R.; Das, N. Silsesquioxane-Based and Triptycene-Linked Nanoporous Polymers (STNPs) with a High Surface Area for CO2 Uptake and Efficient Dye Removal Applications. *Mater. Adv.* **2020**, *1* (9), 3406−3416.
(77) Zhang, A.; Gao, H.; Li, W.; Bai, H.; Wu, S.; Zeng, Y.; Cui, W.; Zhou, X.; Li, L. Hybrid Microporous Polymers from Double-Decker-Shaped Silsesquioxane Building Blocks via Friedel-Crafts Reaction. *Polymer* **2016**, *101*, 388−394.
(78) Wang, D.; Yang, W.; Feng, S.; Liu, H. Constructing Hybrid Porous Polymers from Cubic Octavinylsilsequioxane and Planar Halogenated Benzene. *Polym. Chem.* **2014**, *5* (11), 3634−3642.
(79) Fu, Z.; Mohamed, I. M. A.; Li, J.; Liu, C. Novel Adsorbents Derived from Recycled Waste Polystyrene via Cross-Linking Reaction for Enhanced Adsorption Capacity and Separation Selectivity of CO2. *J. Taiwan Inst. Chem. Eng.* **2019**, *97*, 381−388.
(80) Ravi, S.; Choi, Y.; Park, W.; Han, H. H.; Wu, S.; Xiao, R.; Bae, Y. S. Novel Triazine Carbonyl Polymer with Large Surface Area and Its Polyethylimine Functionalization for CO2 Capture. *J. Ind. Eng. Chem.* **2022**, *108*, 188−194.

https://doi.org/10.1021/acsomega.4c08460
ACS Omega 2025, 10, 2725−2734